

# Decoupled Discrete Current Control for AC Drives at Low Sampling-to-Fundamental Frequency Ratios

Meiqi Wang, *Member, IEEE*, Giampaolo Buticchi, *Senior Member, IEEE*, Jing Li, *Member, IEEE*, Chunyang Gu, *Member, IEEE*, David Gerada, *Senior Member, IEEE*, Michele Degano, *Senior Member, IEEE*, Lie Xu, *Member, IEEE*, Yongdong Li, *Senior Member, IEEE*, He Zhang, *Senior Member, IEEE*, and Chris Gerada, *Senior Member, IEEE*

**Abstract**—Implementation of proportional-integral (PI) controllers in synchronous reference frame (SRF) is a well-established current control solution for electric drives. It is a general and effective method in digital control as long as the ratio of Sampling to Fundamental (S2F) frequency ratio,  $r_{S2F}$ , remains sufficiently large. When the aforesaid condition is violated, such as operations in high-speed or high-power drives, the performance of the closed-loop system becomes incrementally poor or even unstable. This is due to the cross-coupling of the signal flow between d and q axes, which is introduced by the SRF. In this article, an accurate model of current dynamics which captures the computational delay and PWM characteristics in discrete time domain is developed. This motivates the investigation of eliminating cross-coupling effects in PMSM drive systems. A new current control structure in the discrete time domain is proposed targeting full compensation of cross-coupling effects of SRF whilst improving dynamic stiffness at low S2F ratios. The matching simulation and experimental results carried out on a 5-kW high speed drive corroborate the theoretical analysis.

**Index Terms**—DDPI, decoupled current control, discrete-time system modeling, Low S2F tuning method, decoupling

## I. INTRODUCTION

THE drive towards research and development in high-speed electrical drives has seen a rapid growth in the last decade, with an increased technology uptake [1]. Higher speed of electric machines are ones which operate at higher fundamental frequency. This leads to lower value of the

sampling to fundamental (S2F) frequency ratios in digital drive systems, causing substantial dynamic and stability challenges in control systems [2-6].

The design of current regulators in the continuous time domain, with subsequent discretization to get the resulting digital current regulators, has been widely used and proven adequate for most applications. It is usually assumed that the machine fundamental frequency is much lower than the drive sampling and switching frequency, so that the influence of computational delay and discretization errors in digital implementation can be ignored in the design process [2]. However, in high-speed applications, the demand of high fundamental frequencies can lead to significant negative effects of discretization on digital drive system dynamic performance [3], highly oscillatory response, and even instability may occur if the design of current regulator does not aptly incorporate the effects of the discretization of the controllers [4]. Additionally, it is well known that the digital implementation of control systems introduces delays, whose negative effects on dynamic performance also increases with the lower ratio of S2F frequency [5]. Traditional current controllers are implemented in the synchronous reference frame (SRF), the transformation during the delay time introduces additional cross-coupling components to the plant model which is usually ignored and further reduce the system stability [6].

Many researchers have attempted to improve the drive performance at low S2F ratios. State feedback decoupling has been widely used to improve system dynamic performance, but it is not sufficient to guarantee system stability at low ratio of S2F frequency. The internal model control (IMC) proposed in [7] and the complex vector design method introduced in [8] and [9] prompt the robustness of current regulators by implementing zero-pole cancelation to the converted single-input/single-output (SISO) systems, thus enabling higher fundamental frequency operation. Deadbeat and predictive control have been proposed, which provide fast dynamic response with negligible error at steady state [10, 11]. However, even with these attractive attributes, the inherent delay and discretization error of these methods degrade the robustness of the control system and limit the performance at low S2F ratios.

Some research focused on the time delay in the sampling and PWM process, analyzed the bandwidth limitations and compensation methods [4-6, 12-14]. In [12], a delay compensation method in continuous time domain has been proposed, which extended the operation range to a S2F ratio

Manuscript received November 29, 2021; revised March 16, 2022 and May 16, 2022; accepted May 17, 2022. Date of publication; date of current version. This work was supported by the Zhejiang Natural Science Foundation under Grant LY19E070002, Ningbo Science and Technology Bureau under Grant 2022Z019 and the Key International Cooperation of National Natural Science Foundation of China under Grant 51920105011. (*Corresponding author: Meiqi Wang*).

Meiqi Wang, David Gerada, Michele Degano and Chris Gerada are with Power Electronics and Machines and Control (PEMC) research group, University of Nottingham, Nottingham NG7 2RD, UK (e-mail: meiqi.wang1@nottingham.ac.uk; david.gerada@nottingham.ac.uk; michele.degano@nottingham.ac.uk; chris.gerada@nottingham.ac.uk)

Giampaolo Buticchi, Jing Li, Chunyang Gu, and He Zhang are with Power Electronics, Machines and Control (PEMC) research group, University of Nottingham Ningbo China, Ningbo 315104, China (e-mail: giampaolo.buticchi@nottingham.edu.cn; jing.li@nottingham.edu.cn; Chunyang.gu@nottingham.edu.cn; he.zhang@nottingham.edu.cn)

Lie Xu, Yongdong Li are with Electrical Engineering Department, Tsinghua University, Beijing 100190, China (e-mail: xulie@mail.tsinghua.edu.cn; liyd@mail.tsinghua.edu.cn)

Color versions of one or more of the figures in this article are available online at <http://ieeexplore.ieee.org>

Digital Object Identifier

below 10 [13]. A very low S2F ratio control was achieved in further research [13], where an additional model-based error estimator was designed to compensate for the current sampling delay. Several researchers focused on current controllers in discrete time domain to eliminate the cross-coupling effects [15-18]. A very low S2F ratio control was achieved in further research [13], where an additional model-based error estimator was designed to compensate for the current sampling delay. Several researchers focused on current controllers in discrete time domain to eliminate the cross-coupling effects [15-18]. In [16], the effects of different discretization methods have been analyzed and compared, a discrete current regulator based on a symmetric machine model has been proposed, with superior dynamic response compared to continuous-time domain design method being reported. In later research [18], a more comprehensive discrete time-domain system model has been proposed, discrete current controllers considering different sampling methods have been designed, which showed excellent decoupling capabilities at high S2F ratios ( $r_{S2F} \geq 50$ ); however, the decoupling performance degrades at lower S2F ratios ( $r_{S2F} \leq 30$ ). Further, recent publications, e.g. [19] demonstrate that the current control in the rotating reference frame and the associated cross-coupling dynamics are of high scientific and practical relevance and are not yet fully investigated. Although, extensive research has been carried out investigating and developing alternative controllers, current control technique based on proportion-integral (PI) regulators in the SRF is most used, the design and tuning method for low S2F ratio operations is still considered as an interesting research theme and is inadequately reported [20].

This article aims to improve the performance of the current control in d-q reference for low S2F ratio operations. A comprehensive theoretical analysis is provided on the tuning considering the cross-coupling effects in SRF drive system. The focus is on the discrete time domain and complex vector modeling of the variable frequency system. A discrete-time domain system model is developed, that captures the behavior at low S2F ratios and the delays associated with PWM. Compared to the literature that already presents such analysis, i.e., [18], where the stator-voltage output of the inverter is modelled in stator coordinates, this paper provides a more precise discrete time domain model of the system under study by using the rotor coordinates modelling method.

Detailed design procedure is illustrated, by implementing the proposed DDPI to the drive system, the cross-coupling between the flux and torque components is eliminated in transient state. Theoretically, the parameters of DDPI regulators are automatically tuned along with the machines' operational speed and frequency, thus the controller tracking performance is independent of the speed and the S2F ratio. Matching simulation and experimental results carried out on a 5kW high-speed drive corroborate the theoretical analysis.

## II. SYSTEM DESCRIPTION

### A. Complex Transfer Function

Even though the performance of the SRF based PI current regulators may seem intuitive, the multiple-input/multiple-output (MIMO) nature of the system makes its performance

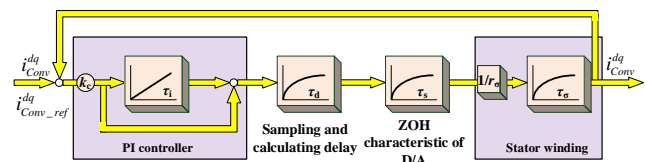


Fig. 1. Simplified model for the current loop of AC machines.

evaluation difficult. The complex vectors are introduced to simplify the model of an AC machine to an equivalent SISO complex vector system. The simplified complex model of the AC machine current loop is shown in Fig 1.

Space vector  $u_{Conv}^{dq}$  is considered as the input, and  $i_{Conv}^{dq}$  is the output variable of the motor. The electromagnetic subsystem can then be described by:

$$i_{Conv}^{dq} + \tau_\sigma \frac{d}{dt} i_{Conv}^{dq} = -j\omega_k \tau_\sigma i_{Conv}^{dq} + \frac{1}{r_\sigma} u_{Conv}^{dq} - \frac{1}{r_\sigma} j\omega_k \psi_f \quad (1)$$

where  $i_{Conv}^{dq}$  and  $\psi_f$  are space vectors that represent the stator current and the rotor flux linkage respectively,  $u_{Conv}^{dq}$  is the stator voltage vector,  $\tau_\sigma$  is the transient stator time constant,  $r_\sigma$  is the stator resistance, and  $\omega_k$  is the angular stator frequency, with all variables normalized by their respective nominal values.

With the feedback cross-coupling decoupling method of back Electro-motive Force (EMF), the plant can be simplified as an inductive-resistive circuit. The transfer function of the permanent magnet motor is derived from (1) as follows:

$$F_P^{dq}(s) = \frac{i_{Conv}^{dq}(s)}{u_{Conv}^{dq}(s)} = \frac{1}{r_\sigma} \frac{1}{1 + s\tau_\sigma + j\omega_k \tau_\sigma} \quad (2)$$

$U_{Conv}^{dq}(s) = \mathcal{L}\{u_{Conv}^{dq}(t)\}$  and  $I_{Conv}^{dq}(s) = \mathcal{L}\{i_{Conv}^{dq}(t)\}$  are the respective Laplace transforms. In the digital control system, the computation and modulation imply an additional delay in the stationary frame  $F_d^{\alpha\beta}(s) = e^{-s\tau_d}$ , where the time constant  $\tau_d$  is the time delay due to the sampling and calculating process [5]. Due to the frequency shift property of the Laplace transform, a generic complex valued vector  $x^{\alpha\beta}(s)$  from the  $\alpha\beta$  stationary reference frame can be transformed into the  $dq$  rotating coordinates  $x^{dq}(s)$  by Park transformation  $x^{dq}(s) = x^{\alpha\beta}(s + j\omega)$ , then the delay resulting from digital signal processing is observed in the SRF as:

$$F_d^{dq}(s) = \frac{u_{Conv,ref}^{dq}(s)}{u_{ref}^{dq}(s)} = e^{-s\tau_d} \underbrace{e^{-j\omega_k \tau_d}}_{\text{cross-coupling}} \quad (3)$$

The typical sample-and-hold characteristic of digital to analog (D/A) conversion for all regular-sampled PWM schemes is the fact that the PWM reference voltage is updated only once per sampling period  $\tau_s$ , which could be addressed by a zero-order-hold (ZOH) element as  $F_{ZOH}^{\alpha\beta}(s) = 1 - e^{-s\tau_s}/s$  in the stationary frame. Then the generic ZOH frequency-domain model at rotating frame is described as:

$$F_{ZOH}^{dq}(s) = \frac{u_{Conv}^{dq}(s)}{u_{Conv,ref}^{dq}(s)} = \frac{1 - e^{-s\tau_s - j\omega_k \tau_s}}{s + j\omega_k} \quad (4)$$

A complete description of all relevant large-signal system dynamics in the continuous time domain is obtained by taking

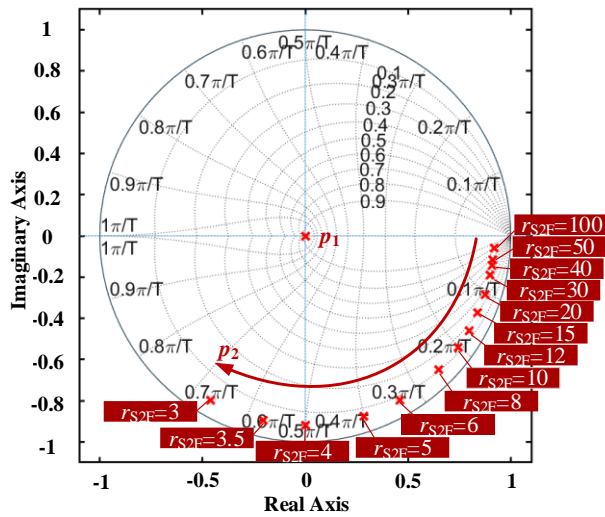


Fig. 2. Pole map of accurate plant model  $r_{S2F}$  (100:1 to 3:1).

the inductive-resistive current dynamics in (2) as well as the sampling, calculation, and D/A transfer characteristics in (3) and (4) into account. Thus, the overall complex-valued transfer function of the system dynamic is:

$$\frac{I_{Conv}^{dq}(s)}{U_{ref}^{dq}(s)} = \underbrace{\frac{1-e^{-s\tau_s-j\omega_k\tau_s}}{s+j\omega_k}}_{\text{ZOH}} \underbrace{e^{-s\tau_d}e^{-j\omega_k\tau_d}}_{\text{S\&C delay}} \underbrace{\frac{1}{r_\sigma(1+s\tau_\sigma+j\omega_k\tau_\sigma)}}_{\text{RL dynamic}} \quad (5)$$

To investigate the cross-coupling effect in discrete time domain, a discrete time-domain equivalent description of a continuous time-domain system transfer function is calculated via the transformation. By introducing the transformation law to (5), an accurate discrete plant model considering the time delay and the transformation from stationary reference frame to rotation reference frame could be obtained:

$$F_{PL}^{dq}(z) = \frac{I_{Conv}^{dq}(z)}{U_{ref}^{dq}(z)} = \mathcal{Z} \left\{ \mathcal{L}^{-1} \left\{ F_{PL}^{dq}(s) \right\} \right\}_{t=k\tau_s} = \frac{K_s \cdot z^{-2}}{(1-\rho_1 z^{-1})} \quad (6)$$

Here,  $\rho_1 = \delta_1 \delta_2$  is one of the plant poles ( $p_1$ ) in complex valued transfer function with  $\delta_1 = e^{-\tau_s/\tau_\sigma}$ ,  $\delta_2 = e^{-j\omega_k\tau_s}$ ,  $K_s = \iota_1 \iota_2$  is the system gain with  $\iota_1 = (1 - e^{-\tau_s/\tau_\sigma})/r_\sigma$ ,  $\iota_2 =$

$e^{-j2\omega_k\tau_s}$ ,  $\mathcal{Z}$  and  $\mathcal{L}^{-1}$  represents the z-transformation and the inverse Laplace-transformation, respectively. Fig. 2 illustrates the pole map of the accurate plant model in the discrete time domain. As it can be seen, the first pole  $\rho_0$  is fixed to the coordinate original of z-domain, while the second pole  $\rho_1$  is varied with the ratios of sampling to fundamental frequency ( $r_{S2F} = f_s/f_e = \omega_s/\omega_k = 2\pi/\omega_k\tau_s$ ). As the ratio reduces, the system pole  $\rho_1$  steps into the left half plane and the system gain  $K_s$  also changes. This matches with the investigation in [12] that converter output errors caused by the rotation in SRF during the time delay, is not only a  $\tau_s$  related phase delay but also a magnitude error of the output voltage.

### B. Cross-coupling effects

It can be noticed from the continuous transfer function in (5), the source of cross coupling is the imaginary coefficients  $j$  which interchanges the signal flow between the real and the imaginary part of the controlled system, i.e.,  $i_q$  and  $i_d$  in a current control system. Moreover, the back EMF generated in the armature winding has an imaginary coefficient which contributes to the cross-coupling effects, as described in (1).

Considering all the above, Fig. 3 illustrates the cross-coupling elements in the current control system with variable values of the electrical angular velocity  $\omega_k$ . Both the delay and ZOH introduce S2F ratio related cross-coupling elements into the SRF control system, and these cross-coupling elements' negative influence increases as the ratio of S2F frequency reducing. As shown in (6), the system pole  $\rho_1$  contains the cross-coupling factor caused by the machine inductance dynamics, while the delay and ZOH caused cross-coupling factor is accommodated in the system gain  $K_s$ . As the operation speed increases ( $r_{S2F}: \infty \rightarrow 1$ ), both system pole and gain move to the left complex plane, with increased magnitude of imaginary parts, which refers to the increasing cross-coupling effects between  $d$ - and  $q$ - axes.

Conventional controllers providing real-valued zero and gain cannot compensate these dynamics of controlled system. With high sampling frequency, the bandwidth of current controller is much higher than the machine fundamental frequency. Thus, the transient-state error is eliminated fast. Even though the cross-coupling exists, it is then compensated after the transient state has faded away. However, in high-performance low-S2F-

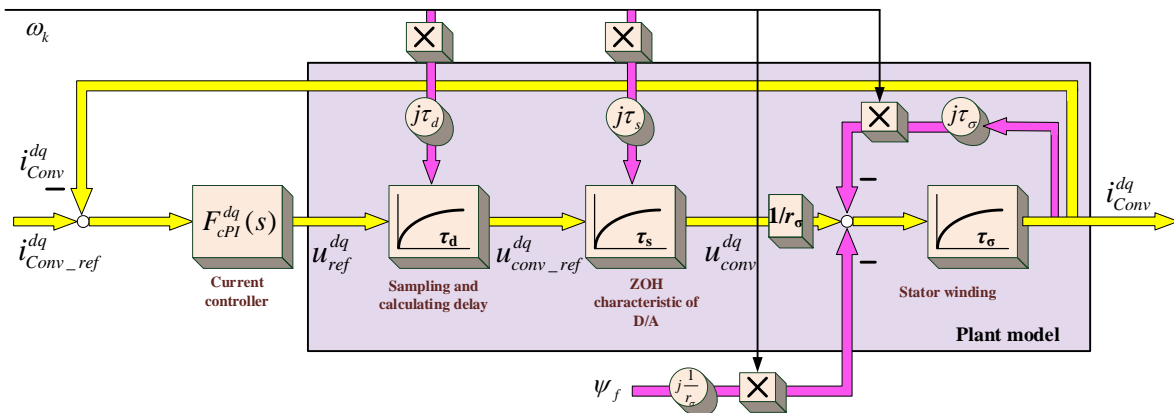


Fig. 3. Current control in synchronous coordinates; accurate machine model; signals that generate cross coupling are marked

ratio drive systems, where controller bandwidth is limited and fast reference tracking ability together with high demand of disturbance rejection are required, the decoupling capability of current controller becomes the key factor driving the overall controller design process. In the following sections, a novel approach to compensate the cross-coupling in the current control system is presented.

### III. SYSTEM DESCRIPTION

#### A. Complex Transfer Function

Synchronous-frame PI current controller, hereinafter referred to as SPI, is conventionally used for independent adjustment of the respective current components  $i_d$  and  $i_q$  in ac drives and grid-tied converters, which achieves reference tracking and disturbance rejection with zero steady-state error. According to the internal model laws [7, 9], it can be defined as:

$$F_{SPI}^{dq}(s) = k_c \frac{(\tau_i s + 1)}{\tau_i s} = \frac{k r_\sigma (1 + s \tau_\sigma)}{s} \quad (7)$$

A common measure to eliminate the cross-coupling effect in the stator winding is to add a feedforward compensation signal to the SPI controller that is mathematically the same as the state feedback control. The compensation signal is intended to cancel the internal motion induced voltage in the stator winding (with imaginary coefficients  $j$  in (2)). By combining the current feedback with gain  $j\omega_k L_\sigma$  added at the output of  $F_{SPI}(s)$ , the imaginary part of the plant pole in  $F_p^{dq}(s)$  could be cancelled, i.e., it replaces the plant transfer function by  $F_p^{dq}(s - j\omega_k) = 1/r_\sigma(1 + s\tau_\sigma)$ . Then, the resulting pole of  $F_p^{dq}(s - j\omega_k)$  is compensated by the zero of controller in (8):

$$F_{SPI}^{dq}(s) \cdot F_p^{dq}(s - j\omega_k) = \frac{k}{s} \quad (8)$$

This method works well for high sampling/switching frequency application, where the practical issues caused by digital implementation process, such as the inverter and sampling delay in (3) and (4), can be neglected. Considering the time delay and the characteristic of D/A, using the Tustin transformation to convert synchronous frame PI current regulator to the discrete domain results in (9), and the close-loop transfer function being (10):

$$F_{SPI}^{dq}(z) = F_{SPI}^{dq}(s) \Big|_{s=\frac{z-1}{\tau_s z+1}} = A \cdot \frac{1}{1-z^{-1}} + B \cdot \frac{z^{-1}}{1-z^{-1}} \quad (9)$$

$$F_C^{dq}(z) = \frac{u_{ref}^{dq}(z)}{i_{Conv\_ref}^{dq}(z)} = \frac{AK_S z^{-2} + BK_S z^{-3}}{1 - (1 + \rho_1)z^{-1} + (AK_S + \rho_1)z^{-2} + BK_S z^{-3}} \quad (10)$$

Where  $A = k_c(1 + \tau_s \tau_i^{-1}/2)$ ,  $B = k_c(\tau_s \tau_i^{-1}/2 - 1)$ . It can be seen from (11) that the poles of close loop transfer function contain  $\rho_1$  and  $K_S$ , which change with the S2F ratio.

#### B. Tuning Methods for SPI Current Controller

It is usually suggested to tune the SPI controller as  $k_c = k l_\sigma$ ,  $\tau_i = \tau_\sigma = l_\sigma / r_\sigma$ , where the controller gain is selected as  $k = 1/2 r_\sigma \tau_s$  and the controller time constant  $\tau_i$  is selected to compensate for the transient stator time constant  $\tau_\sigma$  [6]. In the case of low ratio of S2F, high bandwidth is required to avoid significant oscillation. Researchers established that time delay

is the main limitation for an optimized tuning of the current controllers in terms of desired large bandwidth [5, 14, 21, 22]. In paper [21], the optimized gain tuning method has been suggested to tune PI controller in and, analogously, all forms of linearized ac current regulators by setting:

$$k_c = k l_\sigma \quad (11)$$

$$\tau_i \approx \frac{10}{\omega_{c(max)}} \quad (12)$$

$k$  is the controller gain as well as bandwidth for acceptable damped response, taking into account the  $1.5\tau_s$  delay, the value has been suggested in [21] for maximum bandwidth as  $k_{max} \approx \frac{9.3}{100} \cdot 2\pi f_s$ , where a slightly greater value of 10% is known as an classic rule of thumb for generic digital control applications. While in [20], a simple rule of thumb was proposed by setting the open-loop crossover frequency to 4% of the sampling frequency, as  $k_{opt} \approx \frac{3.9}{100} \cdot 2\pi f_s$ , so that nearly the minimum achievable settling time is achieved in combination with negligible overshoot in the command [20]. The successful results provided by both methods in motor drives have been proved in later works, while the performance at low  $r_{S2F}$  is rarely reported. In this paper, both tuning methods are employed and compared with the proposed DDPI method.

#### C. DDPI Current Controller Design

One should expect to realize the fully decoupled control of machine currents by designing the current controller according to the accurate plant model  $F_{PL}^{dq}(s)$  as established in section II. However, the sampling and calculation delay and ZOH models further complicate the controller structure in  $s$ -domain, which leads to the challenge of digital implementation in digital signal processors. Moreover, the approximation used in controller discretization process leads to incomplete transformation, which degrades the performance of designed controller.

Instead of designing the controller in  $s$ -domain and implementing it in  $z$ -domain, a potential method is directly  $z$ -domain design. Based on the accurate discrete-time domain plant model presented in (6), the decoupled discrete PI (DDPI) current controller implementing zero-pole cancellation

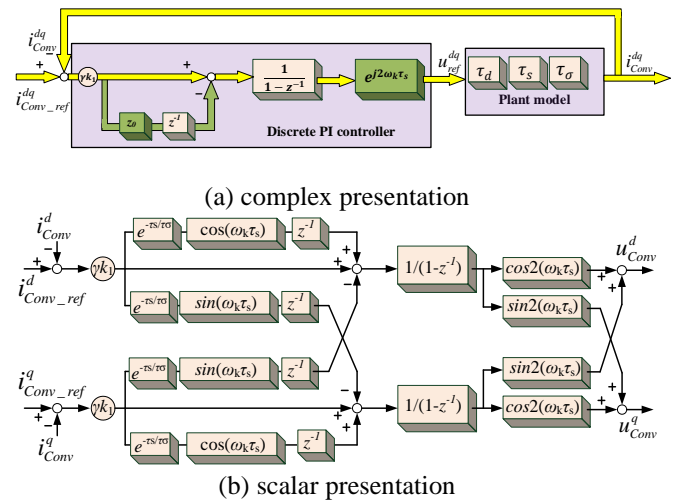


Fig. 4. Structure of proposed DDPI current controller

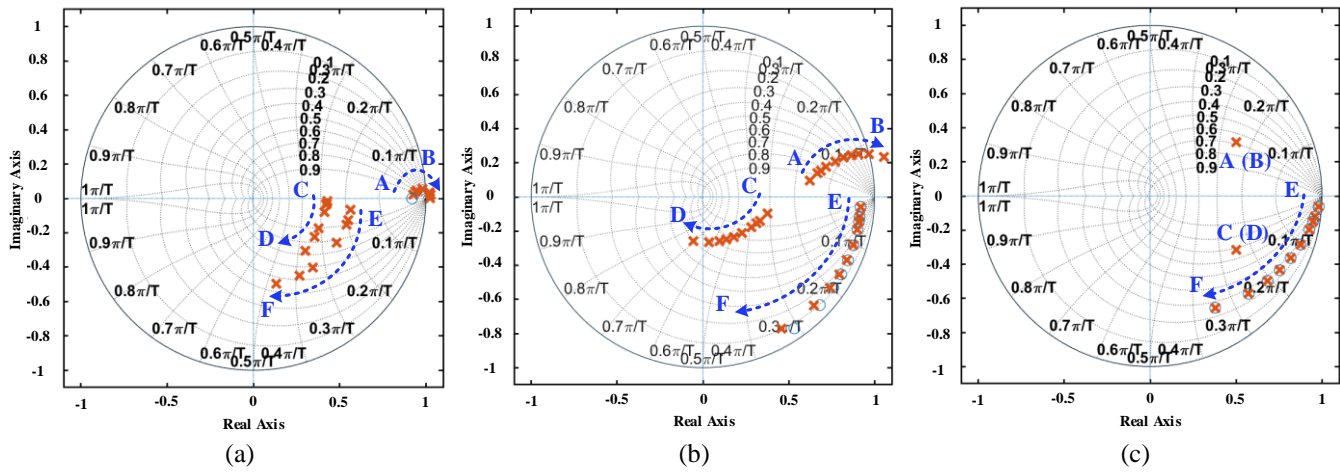


Fig. 5. Close loop zero-pole map of different control strategies ( $r_{S2F}$  from 100:1 to 6:1). (a) SPI without compensation; (b) SPI with feedforward compensation (FC-SPI); (c) DDPI.

principle is proposed. The diagram of the proposed discrete time-domain current regulator is presented in Fig. 4, where the complex and the scalar representation are respectively shown in Fig. 4 (a) and (b).

Similar to the SPI regulators, the basic structure of DDPI should contain both integral and proportional control laws, but it is designed to directly cancel cross-coupling effects of plant  $F_{PL}^{dq}(z)$  in discrete-time domain. Therefore, the structure of discrete-time domain current controller  $F_{DDPI}^{dq}(z)$  is set to:

$$F_{DDPI}^{dq}(z) = K_c \frac{1 - z_0 z^{-1}}{1 - z^{-1}} \quad (13)$$

The controller's zero  $z_0$  is chosen to compensate the highest system response time and the cross-coupling effects caused by the inductor dynamics

$$z_0 = \delta_1 \delta_2 = e^{-\frac{\tau_s}{\tau_\sigma}} \cdot [\cos(\omega_k \tau_s) - j \sin(\omega_k \tau_s)] \quad (14)$$

The complex-valued controller proportional gain  $K_c$  is used to compensate the system gain  $K_s$  for both steady and transient states.

$$K_c = \gamma k_{c1} k_{c2} \quad (15)$$

$$k_{c1} = \tau_\sigma (1 - e^{-\frac{\tau_s}{\tau_\sigma}})^{-1}$$

$$k_{c2} = \cos 2(\omega_k \tau_s) + j \sin 2(\omega_k \tau_s)$$

Here, an additional real-valued factor  $\gamma > 0$  is introduced to shape the command response of the current controller, where  $\gamma \in \mathbf{R}$  is a constant. By implementing the zero-pole cancellation, the cross-coupling terms of the imaginary coefficients  $j$  in the transfer function of (6) have been compensated by the current controller  $F_{DDPI}^{dq}(z)$ . With all single-complex pole of plant model in the  $z$ -domain being cancelled, the open loop transfer function without considering the disturbance resulting from (13) to (15) can be derived:

$$F_{O\_ref}^{dq}(z) = \frac{u_{ref}^{dq}(z)}{i_{Conv\_ref}^{dq}(z) - i_{Conv}^{dq}(z)} = \frac{\gamma z^{-2}}{1 - z^{-2}} \quad (16)$$

It shows no more complex coefficients, thus, the cross

coupling is eliminated theoretically. The close loop transfer function can be obtained as:

$$F_{C\_ref}^{dq}(z) = \frac{u_{ref}^{dq}(z)}{i_{Conv\_ref}^{dq}(z)} = \frac{\gamma z^{-2}}{1 - z^{-1} + \gamma z^{-2}} \quad (17)$$

Comparing (17) with (10), it can be seen, the proposed discrete PI regulator realizes the zero-pole cancellation directly in  $z$ -domain. Both S2F related elements, the plant gain  $K_s$  and the plant pole  $\rho_1$  are compensated by the controller. The comparison of close-loop zero-pole cancellation of different methods is shown in Fig. 5. As shown in Fig. 5(a), the conventional SPI without compensation gets oscillatory as the machine speed increases and becomes unstable (pole adjacent to the boundary of the unit circle migrate toward outside of the unit, point A to B) if the fundamental frequency is bigger than  $f_s/12$ , Whereas, with the feedforward compensation, it can remain stable with fundamental frequency up to  $f_s/8$  as shown in Fig. 5(b). However, there is still a clear tendency of the three single-complex poles to show unbalanced imaginary parts as the angular mechanical velocity increases (A→B, C→D, E→F). As the frequency gets higher, the system pole cancellation zero varies from the pole location (E→F), which cause high frequency oscillation. It is worth to mention that both SPI and feedforward compensated SPI controllers are tuned by  $k_{opt}$  for above analyses, while the similar conclusion is obtained with  $k_{max}$ , a detailed comparison between these two tuning methods will be analyzed in following section. As shown in Fig. 5(c), the proposed controller realizes the fully zero-pole cancellation by setting the cancellation complex zero to the machine's complex pole (E→F). It can realize the fully cross-coupling decoupled control if the back-EMF distortion can be ignored or fully compensated, i.e., back-EMF feedforward compensation is implemented in this paper.

#### IV. ANALYSIS AND VERIFICATION

##### A. Simulation and experimental setup

To verify the proposed DDPI current regulator, simulations are performed within MATLAB/Simulink environment, where

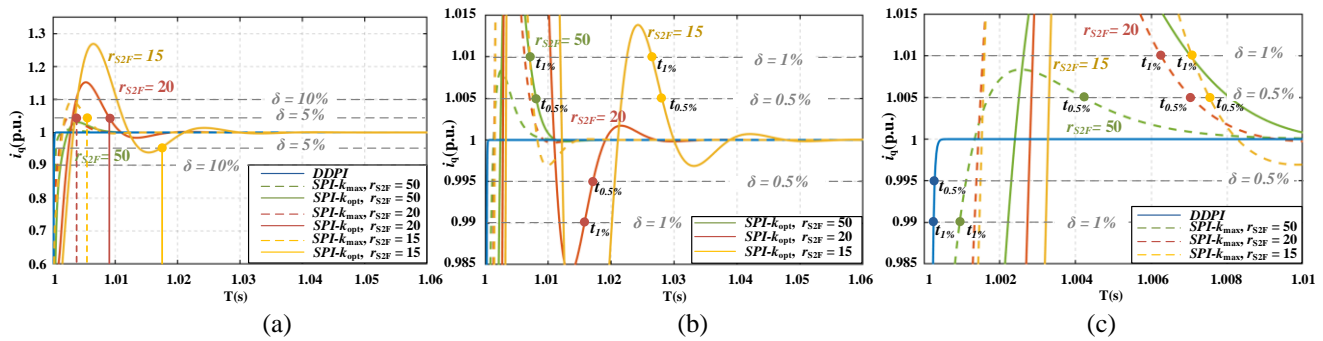


Fig. 6. Q-axis current step response with different sampling to fundamental frequency ratios (50, 20 and 15). (a) General view. Curves with SPI- $k_{opt}$ , SPI- $k_{max}$  and DDPI ( $\gamma = 0.25$ ). (b) Closer view of SPI- $k_{opt}$  plots around  $i_{qref} = 1$  at different  $r_{S2F}$ . (c) Closer view of DDPI and SPI- $k_{max}$  plots around  $i_{qref} = 1$ .

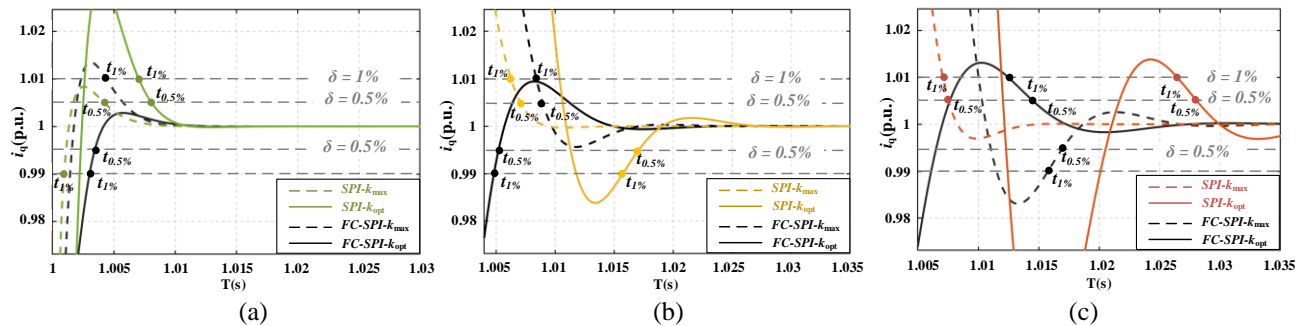


Fig. 7. Q-axis current step response comparison between SPI- $k_{opt}$ , SPI- $k_{max}$ , FC-SPI- $k_{opt}$  and FC-SPI- $k_{max}$ . (a) close view of plots around  $i_{qref} = 1$  at  $r_{S2F} = 50$ . (b) close view around  $i_{qref} = 1$  at  $r_{S2F} = 20$ . (c) close view of plots around  $i_{qref} = 1$  at  $r_{S2F} = 15$ .

a continuous time-domain PMSM model (parameters obtained from experimental test results), an average model of two-level inverter (with one-step delay of output voltage) and a discrete controller have been used. The parameters of test machine are shown in Table I. The validation of the proposed control strategy is also performed on an 120k rpm experimental bench [23, 24]. The setup consists of a high-speed surface-mounted permanent magnet (SPM) machine and a two-level inverter, the switching frequency of the later is set as 10k Hz. The controllers for the experimental tests have been implemented on the designed DSP + FPGA controller board. The single update mode PWM modulation strategy is adopted, and the same PWM frequency and control frequency are used in all simulations and experiments presented in this paper.

TABLE I  
TEST MACHINE PARAMETERS

Parameter	Value	Units
Rated power	5	kW
Rated speed	80k	rpm
Phase resistance	0.67	$\Omega$
Inductance	0.8	mH
Pole pairs	2	/

### B. Results

The overshoot versus settling time trajectories of different methods have been analyzed. A tolerance band of  $\delta = 1\%$  [20] is defined for the settling time. The q-axis current step response associated with each of methods at low sampling to fundamental frequency ratios are represented in Fig. 6. It can be noticed on closely inspecting Fig. 6(b) and (c), that both SPI methods show a degrading tracking performance (setting time more than 5ms, overshoot more than 10%) with decreased S2F ratios (green→red→yellow: 50→20→15), where the solid line presents SPI with tuning method  $k_{opt}$ , dashed line presents SPI with tuning method  $k_{max}$ . It is worth mentioning that for SPI method without the feedforward compensation,  $k_{max}$  tuning method (SPI- $k_{max}$ ) shows a shorter settling time as well as smaller overshoot than  $k_{opt}$  method (SPI- $k_{opt}$ ) for all frequency cases. While, in paper [20], the performance of FC-SPI- $k_{opt}$  and FC-SPI- $k_{max}$  have been analyzed at high ratio ( $\geq 50$ ) applications, where results shows FC-SPI- $k_{opt}$  present a better tracking performance with almost zero overshoot, which is verified as shown Fig 7(a). The performance of FC-SPI and SPI with both tuning methods ( $k_{max}$  and  $k_{opt}$ ) have been compared at low S2F ratios, as shown in Fig. 7(b) and (c).

It is worth to mention that the feedforward compensation method degrades the controller performance rather than improve it with tuning method  $k_{max}$ , where FC-SPI- $k_{max}$  shows larger overshoot and settling time than SPI- $k_{max}$ . The reason is that the intended compensation is counteracted by the inverter and sampling delay at higher angular mechanical velocity.

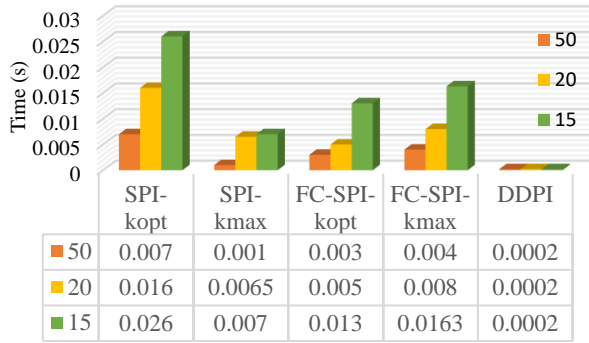


Fig. 8. Settling time (with  $\delta = 1\%$ ) comparison among different methods.

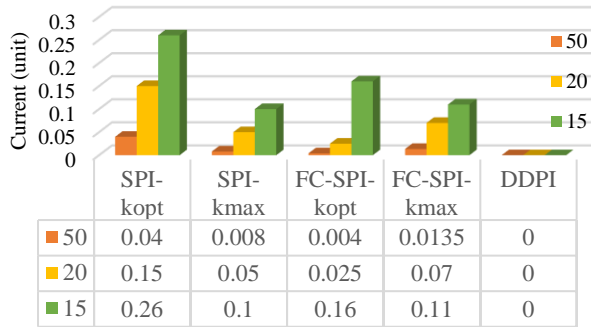


Fig. 9. Overshoot comparison among different methods.

The settling time and overshoot of different methods with reduced S2F ratios have been compared as shown in Fig 8 and Fig9. Among these four exists PI design methods, SPI- $k_{max}$  shows the fastest tracking performance, while SPI- $k_{opt}$  has the worst tracking performance with largest overshoot and longest settling time at all operation frequencies, FC-SPI- $k_{opt}$  shows the smallest overshoot with improved settling time at higher S2F ratios, while the performance degrades at extremely low S2F ratio (i.e.,  $r_{S2F} = 15$ ).

In conclusion, the performance of SPI and FC-SPI controllers varies with the sampling to fundamental frequency.

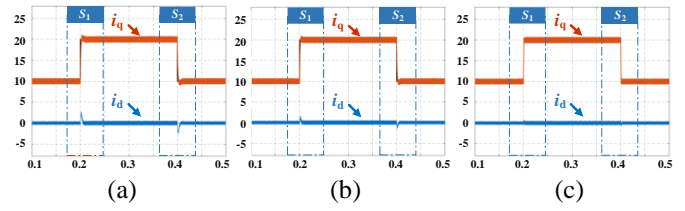


Fig. 10. Command tracking results of different control schemes at 6k rpm,  $r_{S2F} = 50$  and  $f_e = 200\text{Hz}$ . (a) SPI- $k_{opt}$ ; (b) SPI- $k_{max}$ ; (c) DDPI.

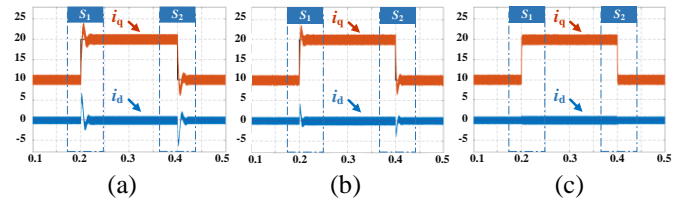


Fig. 11. Command tracking results of different control schemes at 15k rpm,  $r_{S2F} = 20$  and  $f_e = 500\text{Hz}$ . (a) SPI- $k_{opt}$ ; (b) SPI- $k_{max}$ ; (c) DDPI.

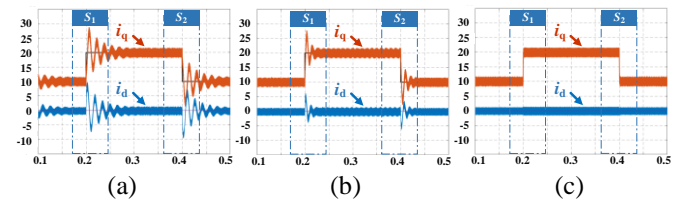


Fig. 12. Command tracking results of different control schemes at 30k rpm,  $r_{S2F} = 10$  and  $f_e = 1\text{kHz}$ . (a) SPI- $k_{opt}$ ; (b) SPI- $k_{max}$ ; (c) DDPI.

Due to the uncompleted decoupling, SPI and FC-SPI controllers face the degraded frequency-dependent tracking performance with increased overshoot and settling time as S2F ratio reducing, whereas a frequency-independent tracking performance with minimum settling time and zero overshoot of the proposed DDPI is shown in Fig. 6, Fig 8 and Fig 9.

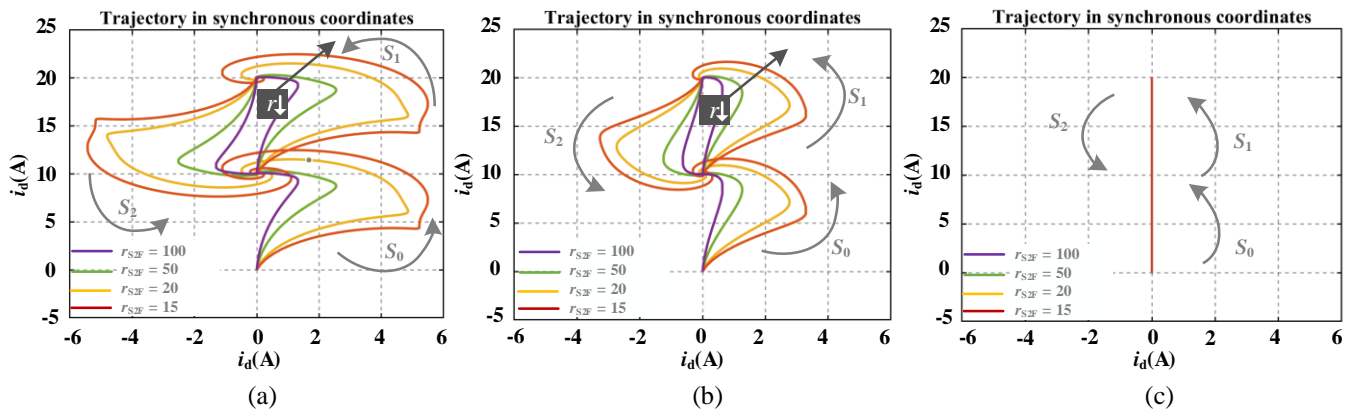


Fig. 13. Recorded Cross-coupling effects of different control schemes with varied S2F ratios ( $r_{S2F} = 100, 50, 20$  and 15). (a) SPI- $k_{opt}$ ; (b) SPI- $k_{max}$ ; (c) DDPI.

The decoupling performance of proposed discrete PI controller has been verified both in simulation and experimental tests. As shown in Fig. 10 to Fig. 12, current step response of the proposed discrete-time domain current regulator is compared to the discrete-time implementation of the SPI. The  $q$ -axis current reference is changed rapidly while the  $d$ -axis reference is fixed as zero. Both SPI methods show overshoots of  $d$ -axis current during the transient state. With fundamental frequency rises from 200 Hz to 1 kHz ( $r_{S2F}$  change from 50 to 10), the overshoot of  $d$ -axis grows fast, which leads to high oscillation of controller output currents. Specifically, SPI- $k_{pot}$  shows a significant overshoot over 50% at 15k rpm ( $r_{S2F}$  equals 20), while SPI- $k_{max}$  shows an improved performance but still

reach the target at 20k rpm ( $r_{S2F}$  equals 15).

The proposed DDPI presents a decoupled control performance (without any  $i_d$  ripple as well as  $i_q$  overshoot during the sudden load change) independent to the ratio of sampling to fundamental frequency, as shown in result (c) of Fig. 10, Fig. 11, and Fig. 12. It is worth to mention that due to the non-linearity of the inverter, a degraded decoupling performance of DDPI occurs at extremely low ratio of 6.67 (operation speed 45krpm), but the current tracking performance is still acceptable. Moreover, the cross-coupling effects (see Fig. 13) of different control schemes under different S2F ratios shows that the current space vector of proposed DDPI is moving along the shortest path between the  $d$ - and  $q$ -axis

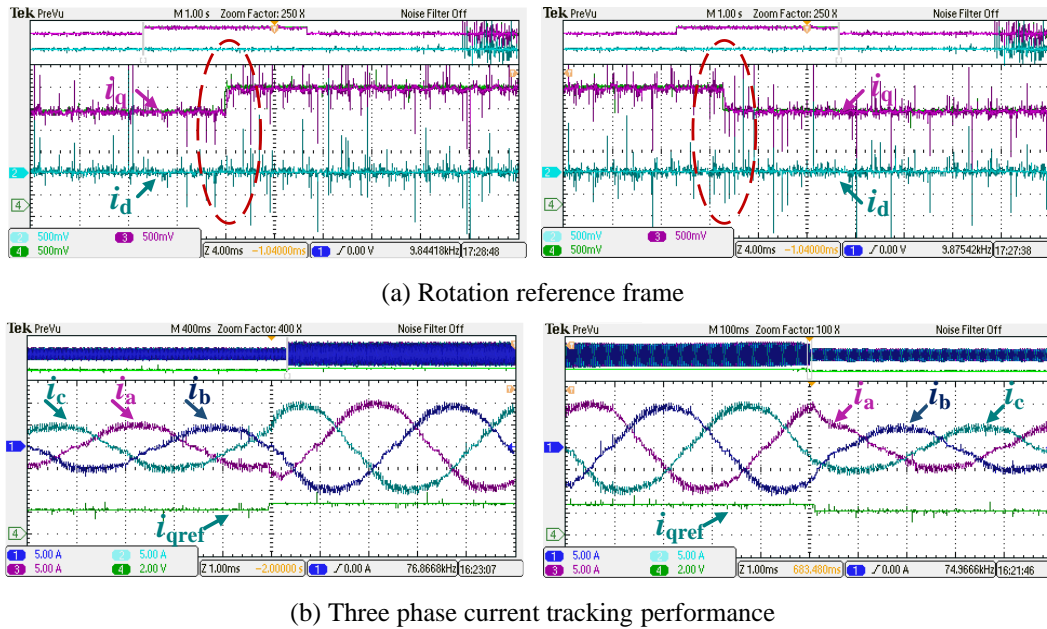


Fig. 14. Transient responses of DDPI at 6k rpm, ratio = 50 and  $f_c = 200$ Hz.

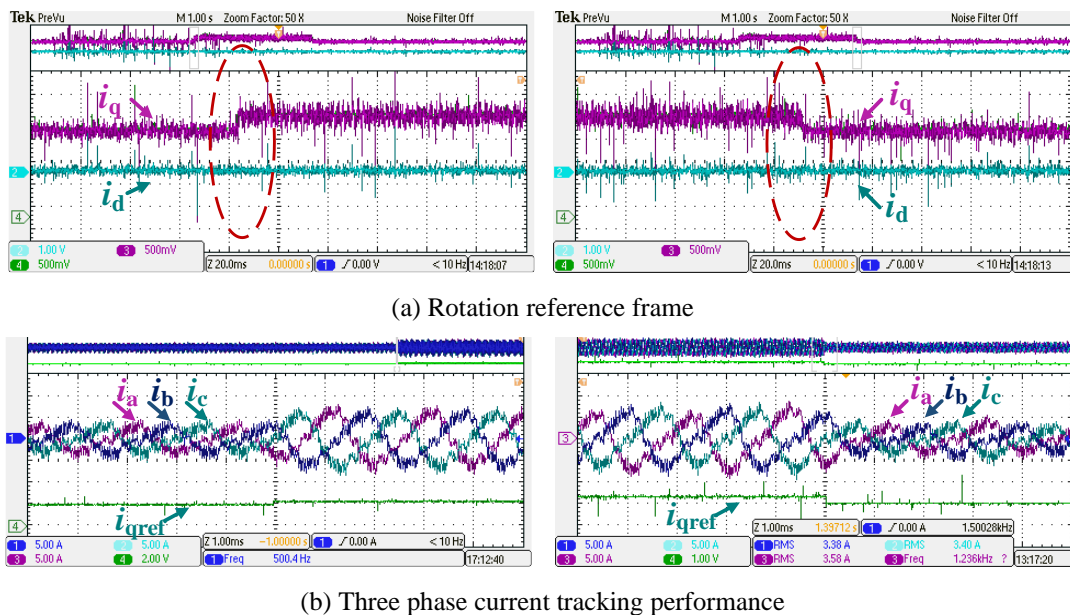


Fig. 15. Transient responses of DDPI at 15k rpm, ratio = 20 and  $f_c = 500$ Hz.

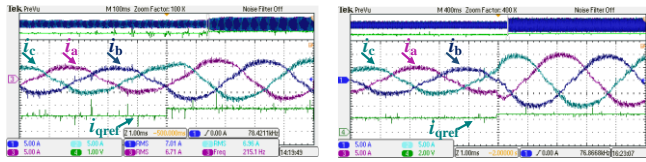


Fig. 16. Step response at 6k rpm, ratio = 50 and  $f_e = 200\text{Hz}$ . (Left - SPI- $k_{\max}$ , right - DDPI).

current commands, which implies the fully decoupled control of the torque and field current components.

The experimental dynamic responses of proposed DDPI are shown in Fig. 14 and Fig. 15. Fig. 14(a) and Fig. 15(a) experimentally verify the simulation results shown in Fig. 10(c) and Fig. 11(c). Fig 14(b) and Fig. 15(b) show the stationary frame three-phase current responses during the transient states. At the beginning of the experiment, the inverter is injecting a current of 5 A per phase. As in the simulation results shown in Fig. 10(c) and 11(c), firstly the current reference  $i_{qref}$  is increased from 10 to 20 A (transient state -  $S_1$ ), and 200ms later, the current reference  $i_{qref}$  is decreased from 20 to 10 A (transient state -  $S_2$ ). Due to the limitation of converter cooling system, a scaled down  $i_{qref}$  is applied in the experimental test. At low frequency verification, current steps from 5A to 10A and then 5A are used, while smaller current references (from 3A to 6A to 3A) are applied in high frequency validations. Since the current is smaller ( $1/10^{\text{th}}$  of the rated current), a relatively higher THD can be observed in the output three-phase current during the high-speed test as shown in Fig. 15(b). However, the fully decoupled current control is still realized and experimentally demonstrated at these reduced current values.

Moreover, the comparison of tracking performance of SPI- $k_{\max}$  and proposed DDPI (Fig. 16) indicates the fast-tracking performance of DDPI, the same conclusion can be also drawn from Fig. 8.

### C. Robustness

Fig. 17 demonstrates the effects of stator resistance mismatches on the step responses of proposed DDPI at a low S2F ratio of 15. In Fig 17 (b), the normal condition with actual resistance  $R = \hat{R}$  has been illustrated as reference, where the system presents decoupled control performance with no oscillation in d-axis current. The same decoupled control performance can be seen in Fig 17(a) with actual resistance  $R = 2\hat{R}$  and Fig 17(c) with actual resistance  $R = 0.5\hat{R}$ .

The effects of stator inductance mismatch on the controlled system are illustrated in Fig. 18 (S2F ratio of 15 is also considered here). The normal condition with actual inductance  $L = \hat{L}$  is presented as reference, shown in Fig. 18(b). It can be seen from Fig. 18 (a) to (c), the decoupled control performance is not affected by the inductance mismatch.

### D. Gain factor impact

As shown Fig. 19, by changing the value of gain factor  $\gamma$ , the influence of the controller proportional gain  $K_c$  to the pole-zero location of the dominant pole-pair is manipulated without affecting the pole-zero locations of other system dynamics. The corresponding damping ratio and natural frequency are presented on the right side of the polar map of Fig. 19. It is worth to mention that higher value of  $\gamma$  leads to reduced

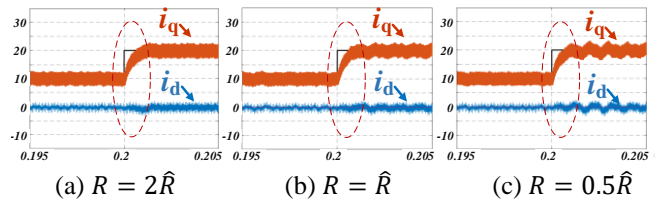


Fig. 17. Current tracking performance under mismatch in the stator resistance

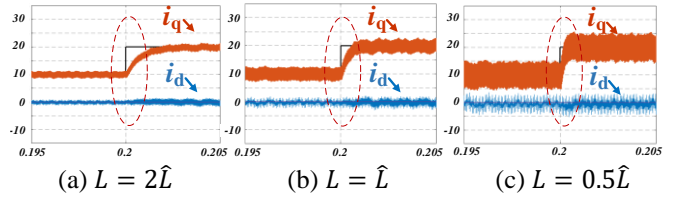


Fig. 18. Current tracking performance under mismatch in the stator inductance

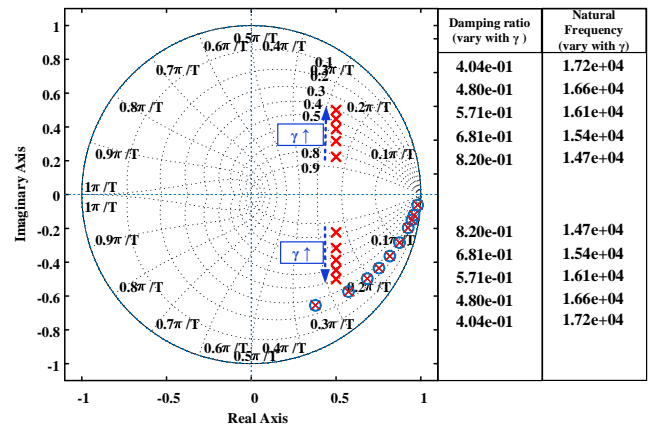
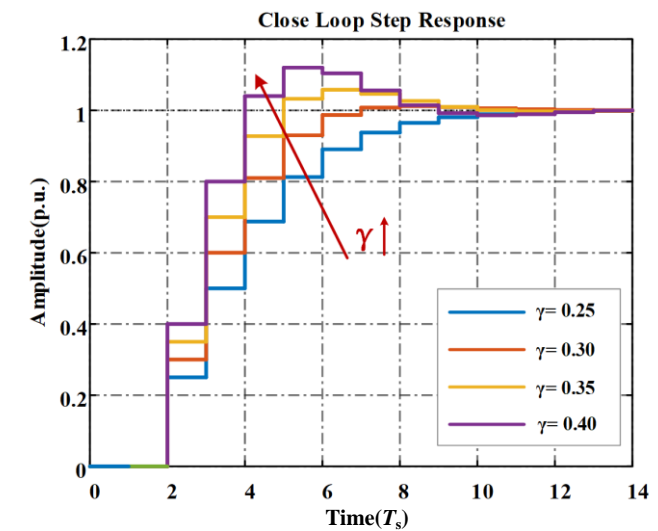


Fig. 19. Close loop polar-zero map of DDPI with varied  $\gamma$



damping ratio and natural frequency, which indicates a fast dynamic response of the system. Fig. 20 shows the step

response of the closed loop control system and the reference for the controller parameter  $\gamma$  selection, in which the controller shows no overshoot current tracking with  $\gamma = 0.25$  and a faster control with  $0.25 < \gamma < 0.5$ .

## V. CONCLUSION

In this paper, the influence of sampling and time delay as well as D/A characteristic of PWM in digital motor drive systems is analyzed, and an accurate discrete plant model capturing the cross-coupling effects in the rotation reference frame is proposed. The accurate model is used to evaluate two existing current control methods as well as the proposed decoupled discrete current controller. Different design methodologies are analyzed in detail and compared. As a result, some important reference guidelines can be drawn as summarized in Table II.

TABLE II  
SUMMARY OF PI DESIGN METHOS

Design method	Pro/Cons
SPI	<ul style="list-style-type: none"> <li>▪ Widely separated current control strategy, the current tracking performance is degraded by the cross-coupling effects caused by the time delay and digital implementation.</li> <li>▪ Considering the cross-coupling effects, <math>k_{\max}</math> is suggested for low S2F ratios applications.</li> </ul>
FC-SPI	<ul style="list-style-type: none"> <li>▪ Mathematically same as state feedback decoupling control methods. Providing improved performance to SPI, however, the performance depending on tuning methods. With the rule of thumb <math>k_{\max}</math>, this method degrades the current tracking performance rather than improve it.</li> <li>▪ Considering the cross-coupling effects, <math>k_{\text{opt}}</math> is suggested for low S2F ratios applications.</li> </ul>
DDPI	<ul style="list-style-type: none"> <li>▪ Directly z-domain decoupled design methods, compensate the cross-coupling effects of rotation reference frame control system.</li> <li>▪ Guarantee tracking performance at fundamental frequency up to 15% of the switching frequency.</li> </ul>

The proposed DDPI targets to cancel the  $r_{S2F}$  dependent cross-coupling effect of rotational frame current control system. Without current and flux observers, the proposed discrete-time domain current controller allows to guarantee tracking

performance at fundamental frequency up to 15% of the switching frequency with respect to the state-of-the-art current control of about 10% [12].

The theoretical analysis presented and simulated in MATLAB/Simulink, is validated by means of experimental measurements performed on a 5-kW high speed drive with the results showing a very close match. The work presented introduces a decoupled PI current control design method that enables improved tracking and dynamic performance with respect to the conventional design methods.

## REFERENCES

- [1] D. Gerada, A. Mebarki, N. L. Brown, C. Gerada, A. Cavagnino, and A. Boglietti, "High-Speed Electrical Machines: Technologies, Trends, and Developments," *IEEE Transactions on Industrial Electronics*, vol. 61, no. 6, pp. 2946-2959, 2014, doi: 10.1109/TIE.2013.2286777.
- [2] Y. Xu, C. Morito, and R. D. Lorenz, "Accurate Discrete-Time Modeling for Improved Torque Control Accuracy for Induction Machine Drives at Very Low Sampling-to-Fundamental Frequency Ratios," *IEEE Transactions on Transportation Electrification*, vol. 6, no. 2, pp. 668-678, 2020, doi: 10.1109/te.2020.2977204.
- [3] A. G. Yepes, F. D. Freijedo, J. Doval-Gandoy, L. Ó, J. Malvar, and P. Fernandez-Comesaña, "Effects of Discretization Methods on the Performance of Resonant Controllers," *IEEE Transactions on Power Electronics*, vol. 25, no. 7, pp. 1692-1712, 2010, doi: 10.1109/TPEL.2010.2041256.
- [4] J. Holtz, Q. Juntao, J. Pontt, J. Rodriguez, P. Newman, and H. Miranda, "Design of fast and robust current regulators for high-power drives based on complex state variables," *IEEE Transactions on Industry Applications*, vol. 40, no. 5, pp. 1388-1397, 2004, doi: 10.1109/TIA.2004.834049.
- [5] M. Lu, X. Wang, P. C. Loh, F. Blaabjerg, and T. Dragicevic, "Graphical Evaluation of Time-Delay Compensation Techniques for Digitally Controlled Converters," *IEEE Transactions on Power Electronics*, vol. 33, no. 3, pp. 2601-2614, 2018, doi: 10.1109/TPEL.2017.2691062.
- [6] J. Holtz, "Complex State Variables as Analytical Tool for Control System Design of Medium-Voltage Drives," *IEEE Journal of Emerging and Selected Topics in Power Electronics*, vol. 8, no. 2, pp. 1824-1832, 2020, doi: 10.1109/jestpe.2019.2960577.
- [7] L. Harnefors and H. Nee, "Model-based current control of AC machines using the internal model control method," *IEEE Transactions on Industry Applications*, vol. 34, no. 1, pp. 133-141, 1998, doi: 10.1109/28.658735.
- [8] F. Briz, M. W. Degner, and R. D. Lorenz, "Analysis and design of current regulators using complex vectors," *IEEE Transactions on Industry Applications*, vol. 36, no. 3, pp. 817-825, 2000, doi: 10.1109/28.845057.
- [9] F. B. d. Blanco, M. W. Degner, and R. D. Lorenz, "Dynamic analysis of current regulators for AC motors using complex vectors," *IEEE Transactions on Industry Applications*, vol. 35, no. 6, pp. 1424-1432, 1999, doi: 10.1109/28.806058.
- [10] X. Zhang, B. Hou, and Y. Mei, "Deadbeat Predictive Current Control of Permanent-Magnet Synchronous Motors with Stator Current and Disturbance Observer," *IEEE Transactions on Power Electronics*, vol. 32, no. 5, pp. 3818-3834, 2017, doi: 10.1109/TPEL.2016.2592534.
- [11] W. Xie *et al.*, "Finite-Control-Set Model Predictive Torque Control With a Deadbeat Solution for PMSM Drives," *IEEE Transactions on Industrial Electronics*, vol. 62, no. 9, pp. 5402-5410, 2015, doi: 10.1109/TIE.2015.2410767.
- [12] B. Bon-Ho and S. Seung-Ki, "A compensation method for time delay of full-digital synchronous frame current regulator of PWM AC drives," *IEEE Transactions on Industry Applications*, vol. 39, no. 3, pp. 802-810, 2003, doi: 10.1109/TIA.2003.810660.
- [13] J. Yim, S. Sul, B. Bae, N. R. Patel, and S. Hiti, "Modified Current Control Schemes for High-Performance Permanent-Magnet AC Drives With Low Sampling to Operating Frequency Ratio," *IEEE Transactions on Industry Applications*, vol. 45, no. 2, pp. 763-771, 2009, doi: 10.1109/TIA.2009.2013600.
- [14] M. Tang, A. Gaeta, K. Ohyama, P. Zanchehtta, and G. Asher, "Assessments of dead beat current control for high speed permanent magnet synchronous motor drives," in *2015 9th International Conference on Power Electronics and ECCE Asia (ICPE-ECCE Asia)*, 1-5 June 2015 2015, pp. 1867-1874, doi: 10.1109/ICPE.2015.7168033.

## IEEE JOURNAL OF EMERGING AND SELECTED TOPICS IN POWER ELECTRONICS

- [15] K. Huh and R. D. Lorenz, "Discrete-Time Domain Modeling and Design for AC Machine Current Regulation," in *2007 IEEE Industry Applications Annual Meeting*, 23-27 Sept. 2007, pp. 2066-2073, doi: 10.1109/07IAS.2007.312.
- [16] K. Hongrae, M. W. Degner, J. M. Guerrero, F. Briz, and R. D. Lorenz, "Discrete-Time Current Regulator Design for AC Machine Drives," *IEEE Transactions on Industry Applications*, vol. 46, no. 4, pp. 1425-1435, 2010, doi: 10.1109/tia.2010.2049628.
- [17] A. Altomare, A. Guagnano, F. Cupertino, and D. Naso, "Discrete-Time Control of High-Speed Salient Machines," *IEEE Transactions on Industry Applications*, vol. 52, no. 1, pp. 293-301, 2016, doi: 10.1109/tia.2015.2478750.
- [18] N. Hoffmann, F. W. Fuchs, M. P. Kazmierkowski, and D. Schroder, "Digital current control in a rotating reference frame - Part I: System modeling and the discrete time-domain current controller with improved decoupling capabilities," *IEEE Transactions on Power Electronics*, vol. 31, no. 7, pp. 5290-5305, 2016, doi: 10.1109/tpe.2015.2481726.
- [19] S. Zhou, Y. Zhang, Z. Liu, J. Liu, and L. Zhou, "Implementation of Cross-Coupling Terms in Proportional-Resonant Current Control Schemes for Improving Current Tracking Performance," *IEEE Transactions on Power Electronics*, vol. 36, no. 11, pp. 13248-13260, 2021, doi: 10.1109/tpe.2021.3080131.
- [20] A. G. Yepes, A. Vidal, J. Malvar, O. Lopez, and J. Doval-Gandoy, "Tuning Method Aimed at Optimized Settling Time and Overshoot for Synchronous Proportional-Integral Current Control in Electric Machines," *IEEE Transactions on Power Electronics*, vol. 29, no. 6, pp. 3041-3054, 2014, doi: 10.1109/tpe.2013.2276059.
- [21] D. G. Holmes, T. A. Lipo, B. P. McGrath, and W. Y. Kong, "Optimized Design of Stationary Frame Three Phase AC Current Regulators," *IEEE Transactions on Power Electronics*, vol. 24, no. 11, pp. 2417-2426, 2009, doi: 10.1109/tpe.2009.2029548.
- [22] D. G. Holmes, B. P. McGrath, and S. G. Parker, "Current Regulation Strategies for Vector-Controlled Induction Motor Drives," *IEEE Transactions on Industrial Electronics*, vol. 59, no. 10, pp. 3680-3689, 2012, doi: 10.1109/tie.2011.2165455.
- [23] F. Savi *et al.*, "High-Speed Electric Drives: A Step Towards System Design," *IEEE Open Journal of the Industrial Electronics Society*, vol. 1, pp. 10-21, 2020, doi: 10.1109/OJIES.2020.2973883.
- [24] D. Gerada, X. Huang, C. Zhang, H. Zhang, X. Zhang, and C. Gerada, "Electrical Machines for Automotive Electrically Assisted Turbocharging," *IEEE/ASME Transactions on Mechatronics*, vol. 23, no. 5, pp. 2054-2065, 2018, doi: 10.1109/TMECH.2018.2849081.



**Meiqi Wang** (Member, IEEE) received the B.Eng. degree in electrical engineering from the Northeast Electric Power University, Jilin, China, in 2014. During 2014 to 2017, she was a joint training master student in electrical engineering of Tsinghua University, Beijing, and Northeast Electric Power University, Jilin, China. She is currently pursuing the Ph.D. degree with the Power Electronics, Machines and Control (PEMC) Group, University of Nottingham, Nottingham, U.K.

Her research interests include power electronics and advanced control techniques for high-speed permanent magnet machines and synchronous reluctance machines for transportation electrification.



**Giampaolo Buticchi** (Senior Member, IEEE) received the master's degree in electronic engineering and the Ph.D. degree in information technologies from the University of Parma, Parma, Italy, in 2009 and 2013, respectively. In 2012, he was a Visiting Researcher with the University of Nottingham, Nottingham, U.K. Between 2014 and 2017, he was a Postdoctoral Researcher and Von Humboldt Postdoctoral Fellow with the University of Kiel, Kiel, Germany. In 2017, he was appointed as an Associate Professor in Electrical Engineering

with the University of Nottingham Ningbo China, Ningbo, China, and as a Head of Power Electronics of the Nottingham Electrification Center. He was promoted to Professor in 2020.

His research focuses on power electronics for renewable energy systems, smart transformer fed microgrids and dc grids for the More Electric Aircraft. He is one of the advocates for dc distribution systems and multiport power electronics onboard the future aircraft. He is author/coauthor of more than 230 scientific papers. Dr. Buticchi is currently the Chair of the IEEE-IES Technical Committee on Renewable Energy Systems and the IES Energy Cluster Delegate. During his stay in Germany, he was awarded with the Von Humboldt Postdoctoral Fellowship to carry out research related to fault tolerant topologies of smart transformers. He is an Associate Editor for the IEEE TRANSACTIONS ON INDUSTRIAL ELECTRONICS, the IEEE TRANSACTIONS ON TRANSPORTATION ELECTRIFICATION, and the IEEE Open Journal of the Industrial Electronics Society.



**Jing Li** (Member, IEEE) received the B.Eng. and M.Sc. degrees (Hons.) from the Beijing Institute of Technology, Beijing, China, in 1999 and 2002, respectively, and the Ph.D. degree from the University of Nottingham, Nottingham, U.K., in 2010, all in electrical and electronic engineering. She was a Research Fellow after graduation with the Power Electronic, Machine and Control Group, University of Nottingham. In 2016, she joined the University of Nottingham Ningbo China, Ningbo, China, as an Assistant Professor, where she is

currently an Associate Professor with the Department of Electrical and Electronic Engineering.

Her research interests include condition monitoring for motor drive systems and power distribution systems, advanced control, and design of motor drive systems.



**Chunyang Gu** (Member, IEEE) received the B.Sc. degree in electrical engineering from the Harbin Institute of Technology, Harbin, China, in 2010, and the Ph.D. degree in electrical engineering from Tsinghua University, Beijing, China, in 2015. In 2015, she went to the University of Nottingham, U.K., where she was a Postdoctoral Research Fellow with the Power Electronics, Machines and Control (PEMC) Research Group. Since 2017, she has been an Assistant Professor with the Department of Electrical and Electronic Engineering and the PEMC

Research Group, University of Nottingham Ningbo China, Ningbo, China.

Her research interests include power electronics for transportation electrification, renewable energy and grid applications, e.g., solid-state transformer, solid-state circuit breaker, multilevel converter topologies and

## IEEE JOURNAL OF EMERGING AND SELECTED TOPICS IN POWER ELECTRONICS

control, application of wide-bandgap semiconductor devices, power electronics in EV, railway, marine, and MEA.



**David Gerada** (Senior Member, IEEE) received the Ph.D. degree in high-speed electrical machines from the University of Nottingham, Nottingham, U.K., in 2012. From 2007 to 2016, he was with the Research and Development Department, Cummins, Stamford, U.K., first as an Electromagnetic Design Engineer from 2007 to 2012, and then as a Senior Electromagnetic Design Engineer and Innovation Leader from 2012 to 2016. At Cummins, he pioneered the design and development of high-speed electrical machines, transforming a challenging

technology into a reliable one suitable for the transportation market, while establishing industry-wide-used metrics for such machinery. In 2016, he joined the University of Nottingham, where he is currently a Principal Research Fellow in electrical machines, responsible for developing state-of-the-art electrical machines for future transportation that push existing technology boundaries while propelling the new technologies to higher technology readiness levels.

Dr. Gerada is a Chartered Engineer in the U.K. and a member of the Institution of Engineering and Technology.



**Michele Degano** (Senior Member, IEEE) received the master's degree in electrical engineering from the University of Trieste, Trieste, Italy, in 2011, and the Ph.D. degree in industrial engineering from the University of Padova, Padova, Italy, in 2015. From 2014 to 2016, he was a Postdoctoral Researcher with The University of Nottingham, Nottingham, U.K., where he joined the Power Electronics, Machines and Control (PEMC) Research Group. In 2016, he joined the University of Nottingham as an Assistant Professor in Advanced Electrical Machines and

appointed as an Associate Professor in 2020 and as a Professor in 2022. He is currently the PEMC Director of Industrial Liaison leading research projects for the development of future hybrid electric aerospace platforms and electric transports.

His main research interests include electrical machines and drives for industrial, automotive, railway, and aerospace applications, ranging from small to large power.



**Lie Xu** (Member, IEEE) was born in Beijing, China, in 1980. He received the B.S. degree in electrical and electronic engineering from the Beijing University of Aeronautics and Astronautics, Beijing, China, in 2003, and the M.S. and Ph.D. degrees in electrical and electronic engineering from The University of Nottingham, Nottingham, U.K., in 2004 and 2008, respectively. From 2008 to 2010, he was a Research Fellow with the Department of Electrical and Electronic Engineering, The University of Nottingham. He is currently an Associate Professor

with the Department of Electrical Engineering, Tsinghua University, Beijing, China.

His research interests include multilevel converters, direct ac-ac power conversion, and multilevel matrix converters.



**Yongdong Li** (Senior Member, IEEE) was born in Hebei, China, in 1962. He received the B.S. degree in electrical engineering from the Harbin Institute of Technology, Harbin, China, in 1982, and the M.S. and Ph.D. degrees in electrical engineering from the Department of Electrical Engineering, Institute National Polytechnique de Toulouse, Toulouse, France, in 1984 and 1987, respectively. Since 1996, he has been a Professor with the Department of Electrical Engineering, Tsinghua University, Beijing, China.

His research interests include power electronics, machine control, and transportation electrification.



**He Zhang** (Senior Member, IEEE) received the B.Eng. degree from Zhejiang University, Hangzhou, China, in 2002, and the M.Sc. and Ph.D. degrees in electrical machines from the University of Nottingham, Nottingham, U.K., in 2004 and 2009, respectively. He was a Research Fellow with the University of Nottingham and the Director of the BestMotion Technology Centre. He moved to the University of Nottingham Ningbo China, Ningbo, China, as a Senior Research Fellow in 2014 and a Principal Research Fellow in 2016. He is currently

the Director of the Nottingham Electrification Centre, Power Electronics, Machines and Control Research Group, University of Nottingham.

His research interests include high-performance electric machines and drives for transport electrification.



**Chris Gerada** (Senior Member, IEEE) received the Ph.D. degree in numerical modeling of electrical machines from the University of Nottingham, Nottingham, U.K., in 2005. He was a Researcher with the University of Nottingham on high-performance electrical drives and on the design and modeling of electromagnetic actuators for aerospace applications. In 2008, he was appointed as a Lecturer in electrical machines; in 2011, as an Associate Professor; and in 2013, as a Professor with the University of Nottingham. He is currently an

Associate Pro-Vice-Chancellor for industrial strategy and impact and a Professor of electrical machines with the University of Nottingham. He has authored or coauthored more than 350 referred publications.

His principal research interest includes electromagnetic energy conversion in electrical machines and drives, focusing mainly on transport electrification. He has secured over £20 M of funding through major industrial, European, and U.K. grants. Dr. Gerada was the Research Chair of the Royal Academy of Engineering in 2013 and also the Chair of the IEEE IES Electrical Machines Committee. He was an Associate Editor of the IEEE TRANSACTIONS ON INDUSTRY APPLICATIONS.